Phase Space Representation and Characteristics of El Niño–La Niña

RISHENG WANG

Recherche en Prévision Numérique, Environment Canada, Dorval, Quebec, Canada

BIN WANG

Department of Meteorology, University of Hawaii, Honolulu, Hawaii

ABSTRACT

The variability of El Niño–La Niña events was analyzed in a low-dimensional phase space, a concept derived from dynamic system theory. The space–time extended EOFs derived from the observed monthly mean SST field over tropical Pacific were used as the basis of the phase space that describes the time evolution of ENSO signals. It was shown that the essential features of the ENSO variability, such as the irregular oscillation, the phase locking to the annual cycle, and the interdecadal changes in its propagation and onset, can be effectively represented by a three-dimensional phase space. The typical El Niño–La Niña life cycle is four years with its mature phases in boreal winter. The intensity of the ENSO signal within one life cycle is closely linked to the frequency of its occurrence (onset). The interdecadal variability of the ENSO signals is characterized by both the intensity and the frequency of occurrence, displaying an irregularity with the gross feature comparable to the regime behavior and intermittency of some low-dimensional chaotic systems.

1. Introduction

One of the primary goals of observational study is deducing certain time-invariant quantities to describe the underlying physical system. Classic statistics provide physical information in terms of means, covariances, etc. The underlying dynamics are often described in the frequency domain in terms of spectral characteristics or in the time domain with the help of some stochastic models. Since the long-time behavior of the atmosphere–ocean coupled dynamics, such as ENSO, is typically a complex of an interplay between periodicity and randomness, the classic approaches cannot precisely characterize the observed or modeled variability, which typically display structured but nonperiodic oscillations. For this purpose, the concepts and ideas developed in recent decades in the field of nonlinear dynamic system theory provide new possibilities (e.g., Eckmann and Ruelle 1985; Abarbanel et al. 1993; Zeng et al. 1993; R. Wang 1994). Here, in contrast to the classic approaches in time or frequency domains or in physical space, the dynamics are studied in phase space (or state space) defined on a prescribed basis (a set of coordinates) that describes the underlying system (e.g., Wal-

lace et al. 1993; Fraedrich et al. 1993; Tziperman et al. 1995; Wang et al. 1995). The time evolution of the underlying system leads to trajectories typically circulating along some manifolds, where each circulation is called an ''orbit.'' In this way, the detailed information about the variability can be derived by analyzing the orbit structures and probability measures in a phase space. This information in turn promotes a conceptual understanding of the underlying system (e.g., Wang and Fang 1996; Wang et al. 1998) and may serve as the basis for theoretical and practical purposes such as the prediction of seasonal climate. The present paper is an application of the phase space analysis to the variability of the atmosphere–ocean coupled system associated with El Niño–La Niña events based on observed monthly mean SST data.

El Niño–La Niña and the associated Southern Oscillation (ENSO) are well-documented phenomena (see, e.g., Rasmusson and Carpenter 1982; Philander 1990; Wright et al. 1988; Deser and Wallace 1987, 1990) and there is a growing understanding of the physical mechanisms (e.g., Neelin et al. 1994; Wang and Fang 1996; references therein). The time evolution of the ENSO displays a complex of phase locking to the annual cycle with a biennial component (Rasmusson et al. 1990), irregular change with 2–7-yr cycle (Trenbenth and Shea 1987), and interdecadal variabilities (Wang 1995a, b; Wang and Wang 1996). Many theoretical studies and model experiments (Vallis 1986, 1988; Zebiak and Cane

Corresponding author address: Dr. Bin Wang, Department of Meteorology, University of Hawaii, 2525 Correa Road, Honolulu, HI 96822-2219.
E-mail: bwang@kukui.soest.hawaii.edu

1987; Chang et al. 1995; Tziperman et al. 1995; Wang and Fang 1996) suggest that the ENSO variability may be characterized by a low-order chaotic attractor with stochastic forcing. The well-known Zebiak–Cane ENSO model (Zebiak and Cane 1987) produces basically a low-order oscillation (Chang et al. 1995). In particular, using a low-order dynamic system model derived from the first principles, Wang and Fang (1996) are able to show the essential characteristics of the ENSO evolution such as the irregularity and phase locking to the annual cycle. The objectives of the present study are concerned with the observational evidences for the ENSO dynamics being a low-dimensional attractor. We basically deal with the derivation of a low-dimensional phase space from observed variables to effectively describe the time evolution of the ENSO, particularly with respect to the observed 2–7-yr variability, interdecadal changes, and the phase locking to the annual cycle.

It is well known that a dynamic system with as low as three nonlinearly coupled variables, hereafter referred to as S_1, can produce chaotic variability whose power spectrum is typically continuous and broadbanded, resembling those obtained from stochastic processes (Lorenz 1963). On the other hand, a complex system with a large (or even infinite) number of degrees of freedom, referred to as S_2, may lead to relatively simple dynamics in terms of low dimensionality due to mechanisms such as nonlinear interaction, self-organization, or phase locking, etc. In many instances, the qualitative dynamics of S_2 with respect to the long-time behavior, such as the probability density distribution in phase space and the associated dimensionality and characteristic exponents, are basically the same as the corresponding dynamic system S_1. Now the question is, can some of the subsystems of the atmosphere–ocean coupled dynamics, which apparently belong to S_2 but display low-frequency variabilities, be expressed by a dynamic model of S_1 with fewer nonlinearly coupled variables such that the qualitative dynamics of S_1 is equivalent to the original S_2? The direct answer to this question may be difficult for many practical issues, as it is not always obvious that such an S_1 does exist, or when it does, it is not often easy to find its exact formalism. However, we can indirectly deduce the static and dynamic characteristics based on observational data derived from S_2 to show whether such an S_1 does exist and what characteristics it possesses. The key to this issue is the embedding theorems (Whitney 1936; Takens 1981; Sauer et al. 1991) and the associated nonlinear time series analysis (see, e.g., Eckman and Ruelle 1985; Sauer et al. 1991; Abarbanel et al. 1993). The embedding theorems promise that, if the asymptotic state of S_2 is on a low-dimensional attractor whose phase space is unknown, one can reconstruct the phase space by collecting a sufficient number of linearly independent observables from S_2 such that the reconstructed phase space is equivalent to the original one in the sense that the metric properties of the S_2 are preserved in the reconstructed one (see

Whitney 1936). In this way, the long-time behavior of the underlying system can be more precisely characterized by its orbit structures and probability measures; the predictability can be analyzed in terms of exponential divergence of nearby trajectories (or sensitive dependence on the initial states) and the prediction of its future behavior becomes a nonlinear (locally linear) extrapolation of the trajectories in a phase space.

In reality, the reconstructed phase space may be only a projection of a part of the original phase space due to the complexity of the underlying system (S_2) and the quality and quantity of the observational data (Sauer et al. 1991; R. Wang 1994 and reference therein). This, however, does not prevent us from using the reconstructed phase space as a good approximation to the reality, considering that all theoretical models are, after all, approximations to reality.

The paper is structured as follows: sections 2 and 3 are devoted to the data and method used in the present study. The analysis results will be presented in sections 4 and 5, followed by concluding remarks in section 6.

2. Data

The data used are the 48-yr (January 1950–December 1997) monthly mean sea surface temperatures (SSTs) over the tropical Pacific (30°S–30°N, 120°E–80°W) interpolated on 5° latitude × 15° longitude grids by Wang (1995a) based on the Comprehensive Ocean–Atmosphere Data Sets (Woodruff et al. 1987) from 1950 to 1992 and the SST analysis data from the National Centers for Environmental Prediction (NCEP) from 1985 to 1996 (Smith et al. 1994). One of the advantages of this dataset is that the meridional structure of the SST is well represented. For comparison, Fig. 1 gives the monthly mean SST for two arbitrary months derived from the dataset of 5° latitude by 15° longitude grid used in the present study (Wang 1995a) and that from the 2.5° latitude × 2.5° longitude grids used in NCEP reanalysis. Note that there is a good agreement between the two datasets. The number of grids $L = 132$ and the time length $N = 576$. Seasonal cycle and the interannual linear trend are removed from each grid, as in Vautard et al. (1996). As an example, Fig. 2 displays two time series derived from regional mean SST based respectively on the grids in eastern (15°S–15°N, 90°–140°W) and western (15°S–15°N, 140°E–180°) Pacific.

It should be noted that, in the present context, the removal of the annual cycle and interannual linear trend does not influence the subsequent analysis. The climate mean annual cycle is a linear part of the attractor. Its removal does not disturb the relative order of the trajectories in phase space and thus does not influence the analysis of the orbit structure, including the impact of the annual cycle on the ENSO. The linear trends are mostly associated with the artificial changes occurring at stations close to the continents. For instance, when we performed the space–time extended empirical or-
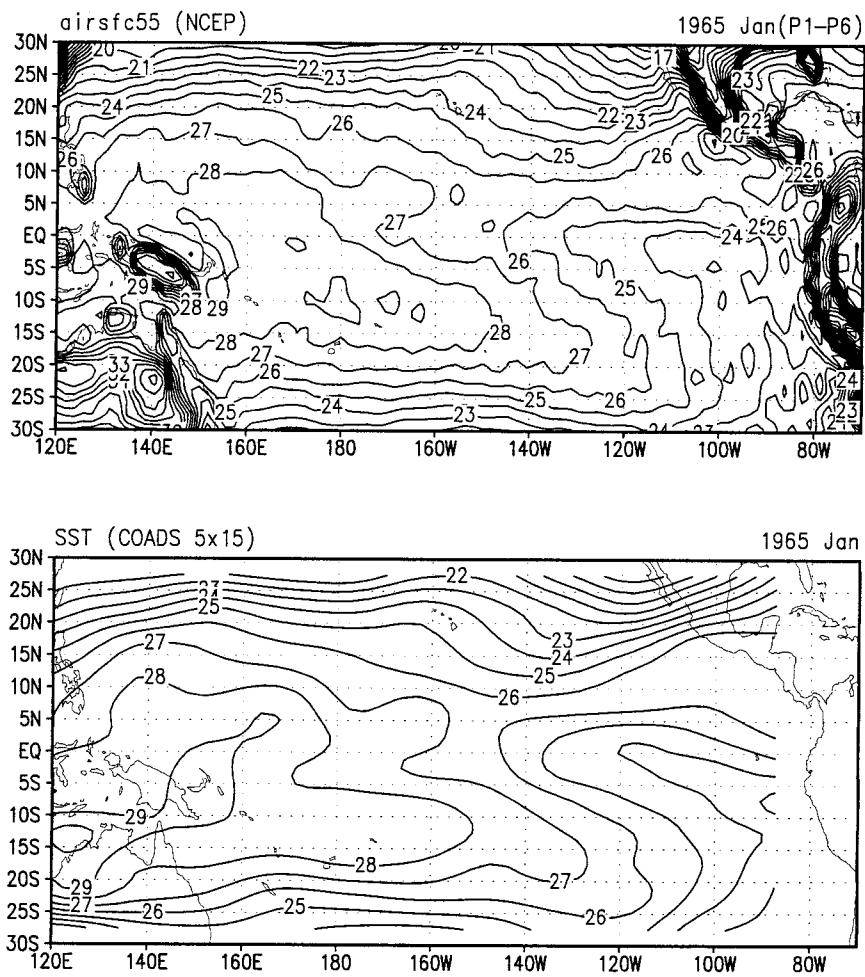
FIG. 1. The monthly SST anomalies derived from tropical Pacific based on 5° lat × 15° long grids (Wang 1995a,b) and 2.5° lat × 2.5° long grids (Reynolds and Smith 1994).
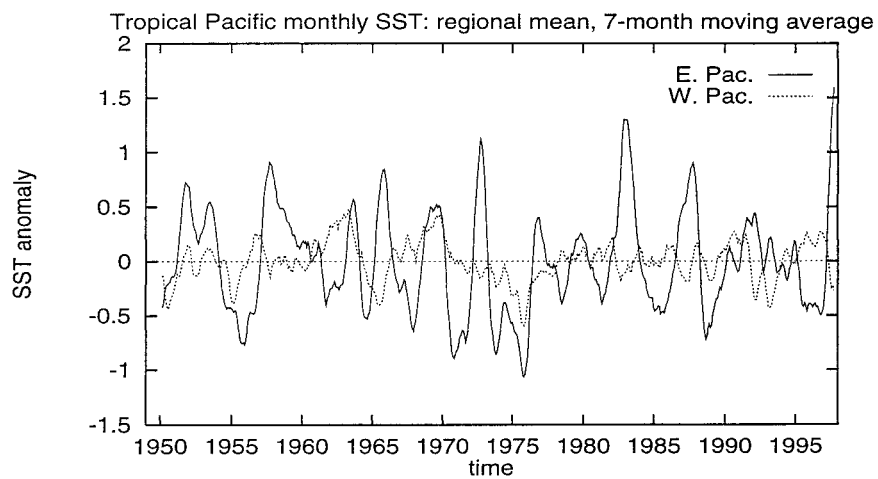

FIG. 2. Reginal mean SST for eastern (solid line) and western (dashed line) tropical Pacific, obtained by avraging between 15°S and 15°N for 90°–140°W and 140°E–180°, respectively. The figure shows their 7-month moving average.

thogonal function (ST-EOF) decomposition without having the linear trend removed, we found that one of the dominant ST-EOF modes appears with the largest anomaly around the northeast corner (close to California) and the southwest corner (close to Australia). The anomalies of all other grids are close to 0. After removing the linear trend, this mode disappeared, implying that, apart from the above-mentioned two regions, the linear trends over all other grids on the tropical Pacific Ocean are negligible. However, it should not be surprising to find a significant linear trend in the long-term mean SST over certain observed period, considering that a linear trend is a part of longer-term fluctuation. Our major concern here is the interdecadal variation of the ENSO that is related to the changes in ENSO life cycle, its intensity, and the frequency of its occurrence.

3. Methodology

a. Phase space reconstruction

The basic ideas of describing the underlying dynamics in phase space are derived from dynamic system theory (e.g., Guckenheimer and Holmes 1983; Eckmann and Ruelle 1985). A dynamic system typically involves a law of motion, Φ, and a phase space (or state space), Ω, such that the state of the system at a given moment t corresponds uniquely to one point in Ω and the time evolution of the states, governed by Φ, results in a trajectory that typically settles asymptotically on a compact subset called the "attractor." The phase space is the coordinate system where the attractor sits. As the dynamics of physical systems often involves wave motions of various kinds, the attractor often resides on some manifolds, parameterized locally by an m-dimensional real vector, $\mathbf{v} \in \mathbf{R}^m$.

In practice, we know neither Φ nor Ω. Typically we have only a limited number of observations, such as temperature, pressure, wind velocity, etc., measured at a fixed sampling interval for a certain time period. Each of the observations can be regarded as an arbitrary real function on Ω such that a real value, x, is assigned to each state. Now the question is, based on the available observations, can we produce a phase space equivalent to Ω in the sense that at least some of the metric properties in Ω are preserved? In terms of dynamic system theory, this is referred to as phase space reconstruction. The theoretical basis for such a possibility is provided by the embedding theorem of Whitney (1936): assume that the asymptotic state of the system is a m-dimensional attractor in Ω; Whitney's embedding theorem states that an Euclidean space, $\mathbf{X} \subset \mathbf{R}^M$, spanned by M linearly independent observations is equivalent to Ω given that $M \geq 2m + 1$ (note that this is a sufficient condition; in reality, M may not need to be larger than $2m + 1$). The equivalence relation implies that the metric properties in Ω are faithfully preserved in $\mathbf{X} \subset \mathbf{R}^M$.

A phase space with such a property is called an "embedding." In this sense, the phase space can be defined as an arbitrary set of coordinates as long as it is an embedding. There are thus many different ways to reconstruct a phase space. In the case of single observable, Takens (1981) shows that a convenient choice for such a set of coordinates is the M linearly independent observations derived from different time lag of the same time series, called time-delay coordinates. In other words, a single time series suffices to produce an embedding of the phase space, given that the time series is sufficiently long (see Smith 1988; Sauer et al. 1991). Figure 3a gives an example of a two-dimensional phase space spanned by a single time series (abscissa) and its seven-month delay (ordinate) derived from the regional mean monthly SST over eastern equatorial Pacific (see Fig. 2). This two-dimensional plane may not necessarily be an embedding, but only a projection of it. Nevertheless, we can still see certain structures of the orbits, particularly the phase locking to the annual cycle by examining how the points are distributed on the plane in Fig. 3a.

As the system under study is spatially extended, the phase space can also be derived from variables observed from different locations of the underlying system. Figure 3b is another example of a two-dimensional phase space spanned by two spatial variables derived from eastern and western equatorial Pacific (see Fig. 2). This is almost the same version as the one with time-delay coordinates (Fig. 3a); however, it is much noisier, has less structure, and has no clear sign of phase locking. Thus the effectiveness of a phase space reconstruction does depend on how it is done. One of the tasks of phase space reconstruction is thus to find a phase space representation that best serves our purpose. Since there is an advantage with the time-delay coordinates, as demonstrated in Fig. 3a, and at the same time, our system is spatially extended, the time-delay techniques of Takens (1981) can be very conveniently extended to multiple variables sampled on grids or at stations. Assume that measurements are taken at L locations over a specific geographical region at an equal time interval τ for a time period of $T = N \times \tau$, leading to a set containing NL-dimensional vectors, extension of Takens's embedding theorem leads to a $M = L \times K$-dimensional Euclidean space where K is associated with the maximum number of time lags. In this way, a given state in the reconstructed phase space, $\mathbf{X} \subset \mathbf{R}^M$, whose elements, $\{\mathbf{x}_t, t = 1, 2, \ldots, N\}$, correspond to a space–time coherent structure within the time window from $t - (K - 1)\tau$ to t in physical space,

$$\mathbf{x}_t = \{x_{l(t-k\tau)}, l = 1, 2, \ldots, L;$$
$$k = 0, 1, 2, \ldots, K - 1\}. \quad (1)$$

Thus the trajectory in $\mathbf{X}$ is equivalent to the changes of the space-time structure with the sliding time window as the time t runs (Fraedrich et al. 1993). This often
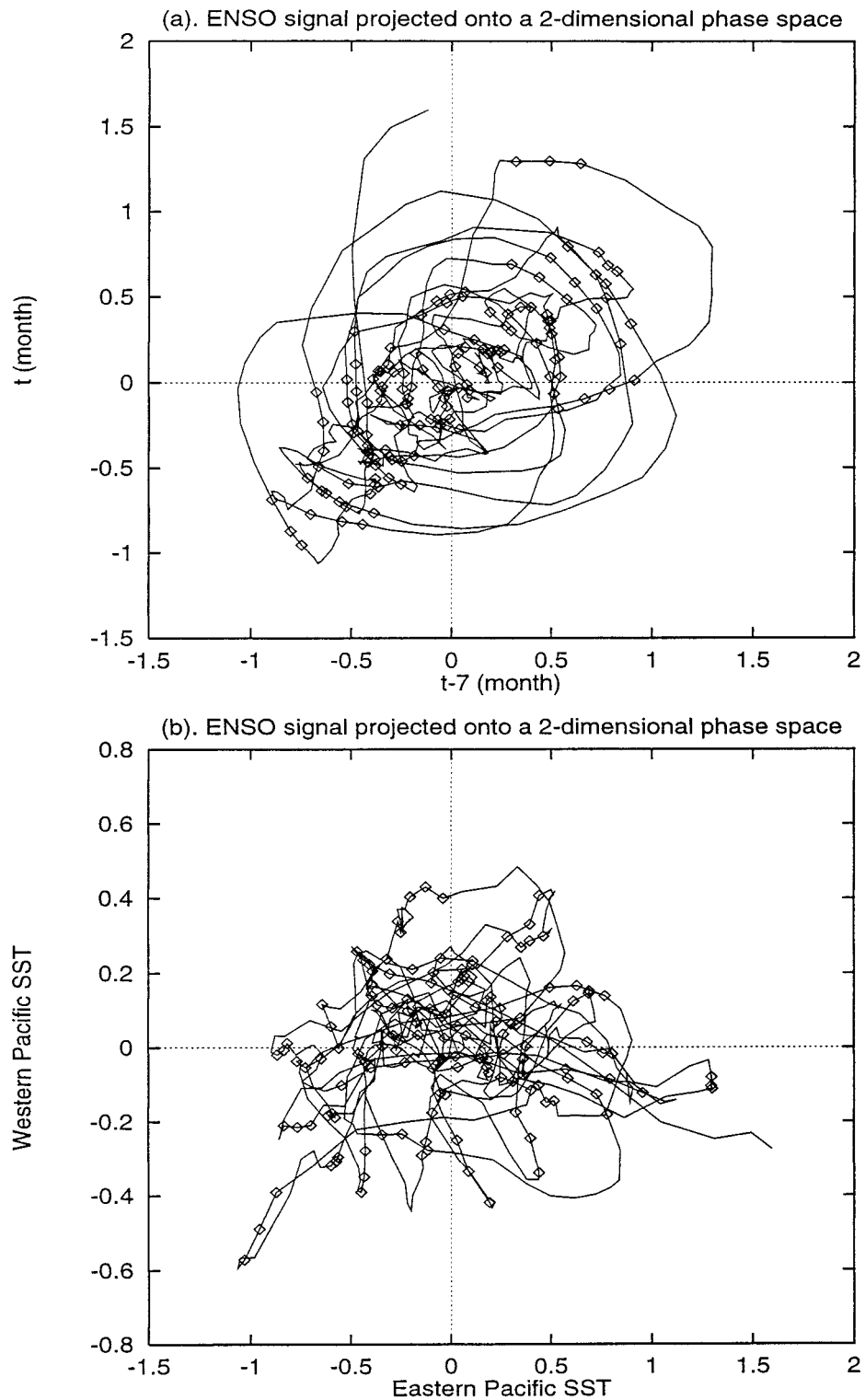
FIG. 3. (a) Two-dimensional phase portrait in the plane spanned by eastern and western tropical Pacific monthly mean SST anomaly derived from Fig. 2. (b) The same as (a) except the plane is spanned by eastern tropical Pacific SST and its 7-month delay. Marked in the figures are also the positions for winter months (DJM) in order to show phase-locking of the ENSO to the annual cycle.

results in a phase space of a rather high dimension, referred to here as the raw phase space.

The choice of the window length K is an important factor to be considered in the present context. For a wavelike motion, K should be chosen around a quarter of the average life cycle. In the subsequent analysis, the maximum time lag of 11 months is used for the time delay coordinates (1), which is equivalent to a time window of $K = 12$ months, close to a quarter of the average ENSO life cycle in physical space. It must be pointed out that the 12-month window is a convenient choice, for that is both the length of the year and around a quarter of the ENSO life cycle. We can guarantee the same qualitative results for windows ranging from 8 months to 2 years.

Application of the $K = 12$ month window to the $L = 132$ spatial variables leads to a $M = 1582$-dimensional phase space, which is apparently too high to be of any practical use. However, not every direction in $\mathbf{X}$ is equally important or meaningful. Hence the task of phase space reconstruction here is reduced to the selection of the subspace $\mathbf{Y} \subset \mathbf{R}^\mu$ from the raw phase space $\mathbf{X} \subset \mathbf{R}^M$, with dimension $\mu \ll M$ that is more relevant to the underlying dynamics. The standard way of reducing the dimension of (1) is the linear transformation of phase space.

b. Phase space transformation

The components of $\mathbf{x} \in X$ may be linearly independent, but they are mostly linearly correlated, particularly when low-frequency variabilities are involved. This can often be eliminated by a proper linear transformation, in particular, by projecting $\mathbf{X}$ onto a prescribed orthogonal basis,

$$\mathbf{y}_t = A\mathbf{x}_t, \quad \text{for } \mathbf{y}_t \in \mathbf{Y} \subset \mathbf{R}^\mu; \quad \mathbf{x}_t \in \mathbf{X} \subset \mathbf{R}^M, \quad (2)$$

where A is a (nonsingular) linear transformation operator or the prescribed basis. In fact, the two-dimensional phase space in Fig. 3 can be regarded as a result of a particular linear transformation of $\mathbf{X}$ for $K = 7$. In this case, the prescribed basis, A, is not orthogonal. Apparently one can design various kinds of A for (2), depending on the purpose of the phase space reconstruction and the data available.

In practice, the purpose of the phase space transformation is to find a suitable projection of the reconstructed phase space such that

- the information contained in the data is condensed in the sense that fewer coordinates are needed to represent the original reconstruction by eliminating the directions corrupted by noise;
- a visual display of a particular subspace is optimized by projecting $\mathbf{X}$ onto its orthogonal basis, since the linear correlation of the coordinates can strongly distort the phase space picture; and
- a possible physical interpretation can be given to the variability represented by a particular subspace.

There are many different kinds of orthogonal basis for $\mathbf{X}$ available (e.g., Broomhead and King 1986; Fraedrich 1986; Sauer et al. 1991). The EOF (empirical orthogonal function) basis, whose advantages cover all the above three criteria, is one of the best choices. The projection of $\mathbf{X} \subset \mathbf{R}^M$ onto its EOF basis is referred to as principal component transformation (Fraedrich and Wang 1993). As the resulting EOFs contain both spatial and temporal dependencies, they are often referred to as ST–EOFs. Projecting $\mathbf{X}$ onto its ST-EOF basis leads accordingly to the space–time principal components (ST-PCs), $\mathbf{Y} \subset \mathbf{R}^\mu$, with μ typically much less than M after the irrelevant directions, in particular those corrupted with noise, are eliminated. Note that the ST-EOF basis is reduced to the standard EOF analysis for $K = 1$. The advantage of the ST-EOF basis over the standard EOFs were demonstrated in Fraedrich et al. (1993) and Wang et al. (1995). As the ST–EOFs contain both spatial variables and time dependence, it is a natural way to represent wavelike motions in the space–time field and thus provide a natural basis for the phase space. The phase space of such a reality as the ENSO derived directly from EOFs would be too noisy to be of practical use.

The EOFs can be directly obtained from the standard procedure of diagonalizing the $M \times M$ covariance matrix derived from (1), as in the extended EOF analysis (Weare and Nasstrom 1982; Wang 1991; Fraedrich et al. 1993). They can also be equally obtained by the procedure of the multichannel singular spectrum analysis (MSSA; Plaut and Vautard 1994), which is mathematically the same as the procedure of the reembedding (Fraedrich and Wang 1993; R. Wang 1994), however, in a different context.

In the standard EOF analysis, one can directly diagnose the $M \times M$ dimensional covariance matrix, where $M = 1582$ in the present instance. This can be directly carried out on larger computers. For smaller computers, one can equally diagnose the $N' \times N'$ time matrix where $N' = N - K + 1 = 553$. In this case, the ST-EOF basis is the standardized principal components (PCs).

In the MSSA (Plaut and Vautard 1994) or the method of reembedding (Fraedrich and Wang 1993; R. Wang 1994), the standard EOF decomposition is applied twice: the first application to the L spatial variables leads to the reduction of the number of spatial variables down to $P \ll K$ PCs, which, in turn, are used for the phase space reconstruction based on (1), instead of the L variables, leading to $M' = P \times K$-dimensional raw phase space. The second application of the standard EOF analysis to this M'-dimensional phase space leads to basically the same results as those directly derived from the M-dimensional one. This procedure is particularly useful when dealing with large L.

The amplitudes and timescales of $\mathbf{y}_t \in \mathbf{Y}$ are determined by the space–timescales of the underlying system. This leads to a separation of different scales (Wang 1991; Fraedrich et al. 1993, Wang et al. 1995). Our

purpose is the selection of a subspace spanned by the relevant ST-PCs in $Y \in \mathbf{R}^\mu$ that describes the time evolution of the system under study. The basis for such a selection is, instead of some mathematical criteria derived from the distribution of the eigenvalues, the physical characteristics of the underlying system in terms of its space–timescales [see R. Wang (1994) for a discussion]. In searching for physical interpretations, one often relies on the examination of the Hovmöller diagram of the ST-EOF patterns, or the cross-time-lagged correlation of the ST-PCs and their power spectra (Fraedrich et al. 1993; Wang et al. 1995). This will be discussed in section 4 in the context of application.

c. Phase space analysis

The phase space reconstruction and phase space transformation are the basic steps for phase space analysis that are aimed at reduction of a phase space that describes the system under study. The purposes of phase space analysis are quantifying the static characteristics and the predictability of the underlying dynamics, understanding their physical implication, and predicting its time behavior (see, e.g., Eckman and Ruelle 1985; Abarbenel et al. 1993).

Phase space analysis can reveal static properties in terms of dimensionality and orbit structures that are impossible for classic time series analysis. For instance, power spectrum analysis of a scalar time sequence, $\{x_i, i = 1, 2, \ldots, n\}$, can show whether a system is periodic or quasiperiodic (torus with basic frequencies, $\{\omega_i, i = 1, 2, \ldots, m\}$). However, for systems with broad continuous spectra, which is often the case for the observed climate variables, it is difficult to get any new information unless the underlying dynamics is a truly random processes. Climate systems are often broadbanded but are not necessarily random processes. The ENSO phenomenon is one of the striking examples (e.g., Tziperman et al. 1995; Wang and Fang 1996; Jin et al. 1994). The differences between stochastic and chaotic dynamics can be most clearly seen from the orbit structure and the associated probability density distribution in phase space. Structured variability can often be embedded or well approximated in a low-dimensional phase space while this is impossible for stochastic process; the structured variability often occupies only a portion of the phase space, that is, the trajectory visits one part of the space more often than others, leading to low-frequency fluctuation and regime behavior, which is not often the case for random process. In the present context, since each point in the phase space corresponds to a space–time structure of the climate variables in physical space, one may be able to give a physical interpretation to the observed variability. Thus analysis of the orbit structure of a dynamic system is very important part of phase space analysis that may lead to further understanding of the nature of the underlying system, such as the dimensionality, aperiodicity, regime behavior, phase locking, etc.

4. Phase space representation

a. The ST-EOF basis

From all the ST-EOF components, we found that the first three leading PCs are the most relevant to ENSO dynamics in space scales and timescales. Figure 4 gives their spatial patterns at time lag 11, 8, 4, and 0 months, respectively. The ST-EOF patterns are basically space–time correlated structures of the physical reality. In the present context, they are used as an orthogonal basis for the phase space where the ENSO signals sit. For convenience, the ST-EOFs will be denoted hereafter by $V = (v_1, v_2, v_3)$. The corresponding ST-PCs, denoted by $Y = (y_1, y_2, y_3)$, are derived by substituting A in (2) with V.

The first ST-EOF (v_1) reflects the mature phases of the ENSO life cycle. The westward propagation of SST anomalies is a common feature of the majority of the basinwide warm and cold episodes. Scrutiny of the equatorial SST anomalies across the basin indicates that among the 13 warm events during the period 1950–97, there are only two with SST anomalies propagating eastward (1963 and 1982–83) and two stationary (1986–87 and 1991–92), whereas the other events show evident westward propagation (Wang 1995b). The derivation of the canonical ENSO warming in Rasmusson and Carpenter (1982) was based on six major El Niño episodes during 1950–77 that exhibit dominant westward propagation: the SST anomalies shift from the far eastern equatorial Pacific on the onset phase (boreal spring of El Niño year) to the central equatorial Pacific on the mature phase (boreal winter of El Niño year). Figure 4a shows that v_1 is dominated by a positive SST anomaly along the eastern and central equatorial Pacific while the center of anomaly travels slightly westward with time. The corresponding ST-PC (see Fig. 5a) coincides very well with El Niño or La Niña years for maximum or minimum y_1, which is highly correlated with the regional mean monthly SST over eastern equatorial Pacific (cf. Fig. 2, solid line). Thus the evolution of v_1, apparently associated with the mature phase of El Niño and La Niña, agrees well with the canonical ENSO and reflects the dominant feature in phase propagation of the El Niño–La Niña episodes that occurred in the 48-yr records.

The second ST-EOF (v_2) represents the transition phases of the ENSO life cycles. In contrast to v_1, v_2 (see Fig. 4b) is characterized by a reverse of sign in the SST anomaly: the positive anomaly in the equatorial central Pacific at time lag 11 months travels westward and at the same time declines in intensity; soon after it has disappeared at lag 6, a negative anomaly center appears off the Ecuador coast. The latter then intensifies with the size of the anomaly center expanding westward
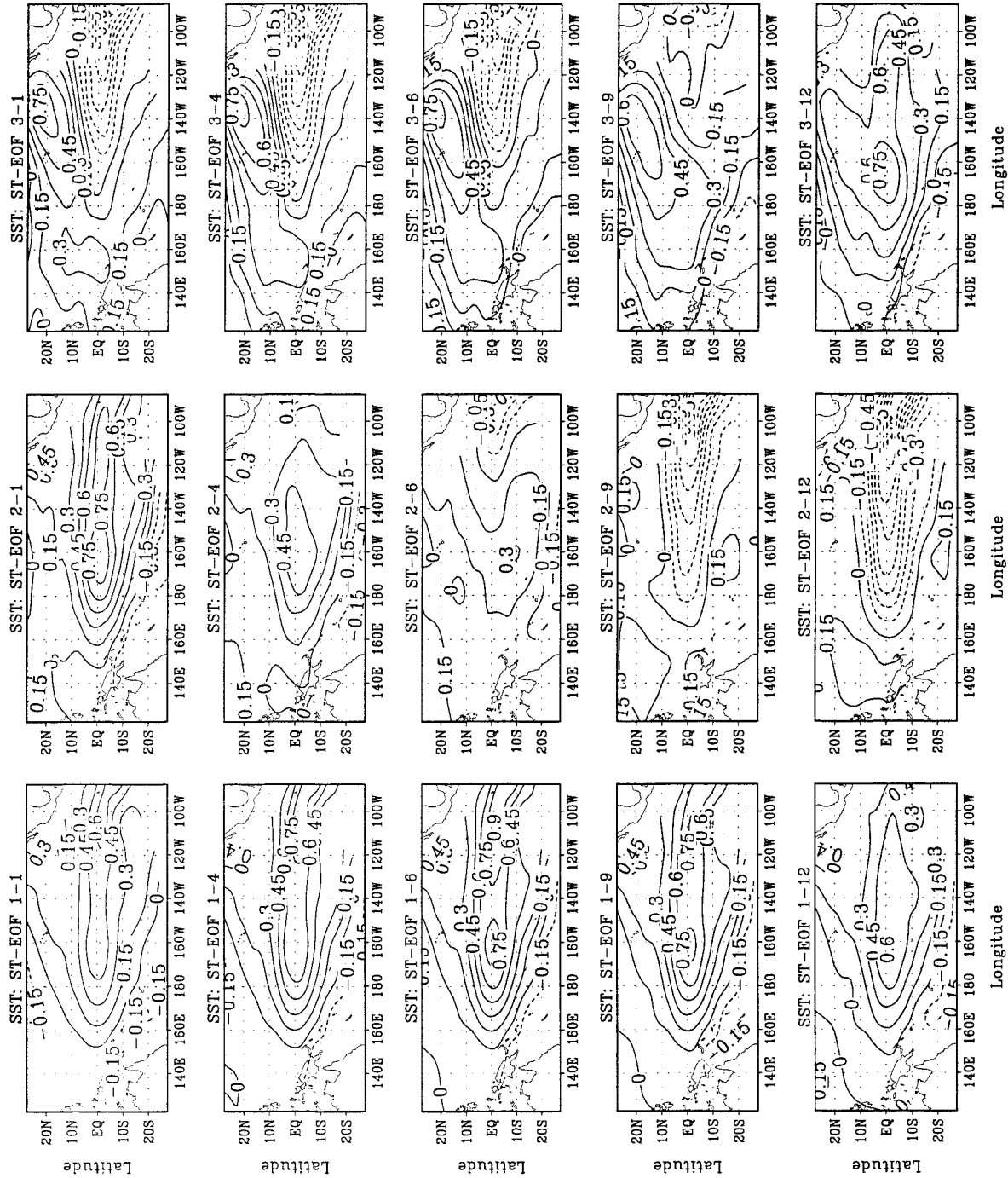
FIG. 4. The spatial patterns of the first three ST-EOFs (v_1, v_2, v_3) at different time lags 11, 7, 4, and 0. The EOF values are standardized to maximum 1.0.
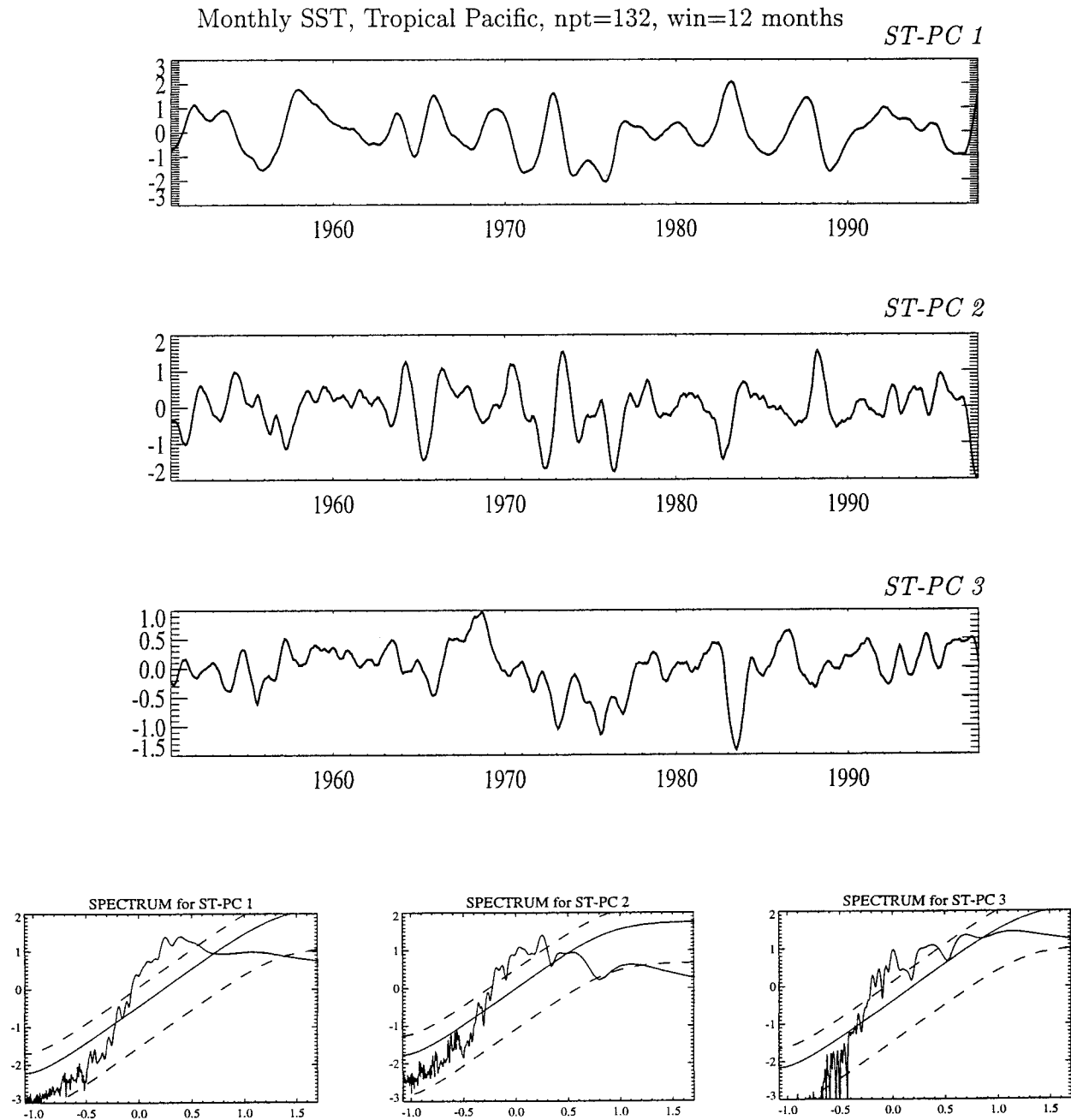
FIG. 5. The first three leading ST-PCs (y_1, y_2, y_3) derived from the projection of the monthly tropical Pacific SST (after seasonal cycles and interannual trends are removed) onto the corresponding ST-EOFs in Fig. 4. The right panel shows their power spectra.

all through lag 0. Apparently, v_2 reflects the change in the ENSO cycles from a warm to a cold phase, when y_2 is positive and vice versa. This can be confirmed from the phase delay of y_2 relative to that of y_1 (Fig. 5), which can also be seen from the lag correlation shown in Fig. 6a. The time series of y_2 exhibits the same characteristic period as y_1, as shown by their power spectra (Fig. 5, lower panel). The difference between y_1 and y_2 lies in that the evolution of the latter involves a

substantially shorter timescale, implying that the transition phases are much quicker than the mature phases.

The third ST-EOF (v_3) is associated with the interdecadal variations of the ENSO signals. Figure 4c shows that v_3 displays a distinctive spatial pattern with a complex time change. The complex evolution pattern of v_3 may be conveniently decomposed into three components: one stationary and two transients. The stationary component consists of a positive SST anomaly of a
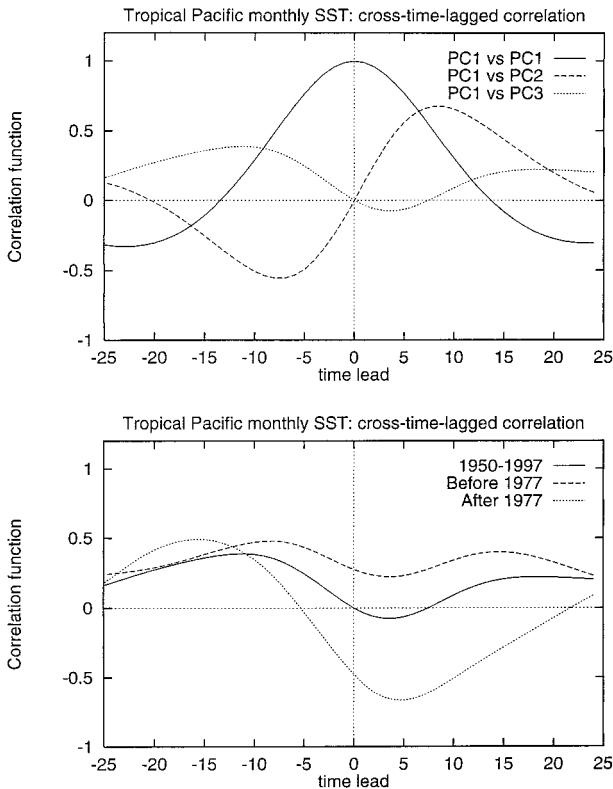
Tropical Pacific monthly SST: cross-time-lagged correlation

Tropical Pacific monthly SST: cross-time-lagged correlation

FIG. 6. (a) Autocorrelation of y_1 (solid line) and its cross-time-lagged correlations with y_2 (dashed line) and y_3 (dotted line). (b) The cross-time-lagged correlations between y_1 and y_3 calculated based on data before (dashed line) and after (dotted line) 1977.

horseshoe shape, emanating from the equator near the date line to the North and South American coasts, respectively. This component is nearly symmetric about the equator and persists all the time during the 12-month period of the time window. Superposing on this stationary horseshoe pattern are the two transient components: the first transient component is antisymmetric about the equator. This one has a large amplitude to the north wing that intensifies and expands equatorward during the 12-month course, and by lag 0 a prominent positive center forms in the equatorial central Pacific. The second transient component is trapped in the equatorial Pacific, characterized by a negative SST anomaly in the equatorial eastern Pacific that persists in the first 5 months, then decays while moving eastward, and is finally replaced by a positive SST anomaly. For convenience, we will refer the three components as the stationary, antisymmetric, and eastward components, respectively. The transient antisymmetric and equatorial eastward components describe the anomalous onset of the ENSO; its function depends on the phase relation with y_2, that is, whether y_3 is nearly in or out of phase with y_2. We shall show later that this is an important part of the interdecadal variabilities.

The interdecadal variability is not much related to the interannual linear trend, as the latter, when there would

be any in the data, is removed from the SST time series (see section 2). Therefore, by looking at the time series of y_3 (Fig. 5, the third panel from the top) or its power spectrum (Fig. 5, lower panel), it is hardly convincing that v_3 related with the interdecadal components of the ENSO variability, although y_3 displays more or less larger-scale variations superposed with fluctuations relevant to the typical ENSO timescale (seen also its spectrum). The interdecadal variability becomes apparent only when examining the phase relation of y_3 with y_1 and y_2, and the changes in the typical ENSO life cycle, the intensity, and the frequency of its occurrences (intermittency; see section 5c).

The interdecadal component is particularly associated with the stationary horseshoe anomaly (Wang 1995a), which is similar to the decadal shift around 1977 found in Nitta and Yamada (1989). Figure 6b gives the cross-time-lagged correlation between y_1 and y_3 using data before and after 1977. Note that there is a significant difference. This will be discussed in more detail in section 5c with respect to regime behavior of the ENSO variability.

The other two transient components display an evolution on the typical ENSO timescale, consistent with the shorter dominant timescales, as are observed from y_3 or its power spectrum (see Fig. 5). On this timescale, y_3 leads y_1 by about 11 months (Fig. 6a). In contrast, the correlation with y_1 leading y_3 is rather insignificant and, if any, at shorter lead time. On the other hand, significant correlation can be observed between y_2 and y_3 on the typical ENSO scales. However, this relation displays an in-phase and out-of-phase change on the interdecadal scales. On average, y_2 and y_3 are in phase before 1977 and out of phase after 1977.

Therefore, given the decadal change in y_3, it is clear that, after 1977, the onset of the ENSO involves an equatorward propagation that is more tied to the Northern Hemisphere SST anomalies toward the equatorial central Pacific. The pre-1977 ENSO has mostly just the opposite transient components whereby the westward propagation along the equator described by the first two ST-EOF modes is enhanced. These features reveal the change of ENSO onset characteristics on interdecadal timescales. The results here are in harmony with the findings of Wang (1995a), who showed the difference in the onset phase of ENSO before and after 1977.

b. Phase–space representation

The foregoing discussions about the characteristics of the ST-EOFs help establish a connection between the dynamics of the ENSO signals in physical space and their phase space representation. The time evolution of the ENSO-related SST, which is reflected by a continuous change of its space–time structure in physical space, corresponds to a trajectory in the three-dimensional phase space spanned by $V = (v_1, v_2, v_3)$. It should be pointed out that the choice of these three coordinates has nothing to do with an arbitrary truncation of the ST-

EOFs. The basic principle for such a choice is that they describe the same manifolds containing the ENSO signals. The above analysis in physical space has provided evidence for these three ST-EOFs being the basis for the subspace that describes the ENSO dynamics. Further evidence can be derived from the relationship between ST-PCs. Figure 6a gives the autocorrelation coefficient (solid line) of y_1 as well as its cross correlation with y_2 (dashed line) and y_3 (dotted lines) as a function of lead time. Indeed, significant correlation is observed between y_1 and itself at time lag (lead) of 2 yr (about half of the average ENSO life cycle) and with other two components at a time lag (lead) of about 6 months to 1 yr, indicating a time shift of about a quarter of the averaged ENSO cycle. In particular, the time-lagged cross correlation between y_1 and y_2 shows a nearly perfect sine function within one life cycle of the ENSO, as is expected from a typical wave motion with intrinsic aperiodicity. Moreover, the time shift between y_1 and y_2 is, in fact, shorter than a quarter of the typical ENSO life cycle because the mature phase takes a longer time than the transition phase (see Fig. 6, dashed line). Accordingly, the orbit structures of the trajectory in the phase space spanned by these two ST-EOFs, shown in Fig. 7a, display a regularity that is expected from a typical wave motion in physical space. However, this regularity is comparable to a linear wave in terms of symmetry only within one ENSO life cycle because each cycle here is different from the others, a typical feature inherent to the irregularity of the ENSO dynamics (see section 5c for details).

There is an apparent asymmetry of the cross-lagged correlation between y_1 and y_3 with respect to 0 lag (Fig. 6a): the maximum correlation occurs between time lag 20 and 10 months while there is no significant correlation with time lead. We found that this is related to the interdecadal change or regime behavior of the ENSO. To understand this, Fig. 6b gives the same correlation function as Fig. 6a for y_1 and y_3 except that the calculation is based on data before (dashed line) and after (dotted line) 1977. Note that there is an apparent difference: before 1977, the ENSO evolution is dominated by normal westward propagation and the contribution from v_3 is not significant, as the couple (v_1, v_2), together with their ST-PCs, describe the normal ENSO time evolution. Apparently, the eastward propagation of the SST anomaly during 1982–83 is associated with v_3, as reveal by the correlation pattern between y_1 and y_3 in Fig. 6b, which is consistent with the foregoing analysis in physical space. This asymmetry is also reflected in the orbit structure of the trajectory in the three-dimensional phase portrait, as shown by its two-dimensional projection onto the plane spanned by v_1 and v_3 in Fig. 7b. The trajectory evolves mostly above the plane $y_3 = 0$ but rarely goes far above. However, it may have large excursions below the plane occasionally. This happened, for instance, during the periods of 1974–75 and 1982–83, when extraordinary La Niña and El Niño
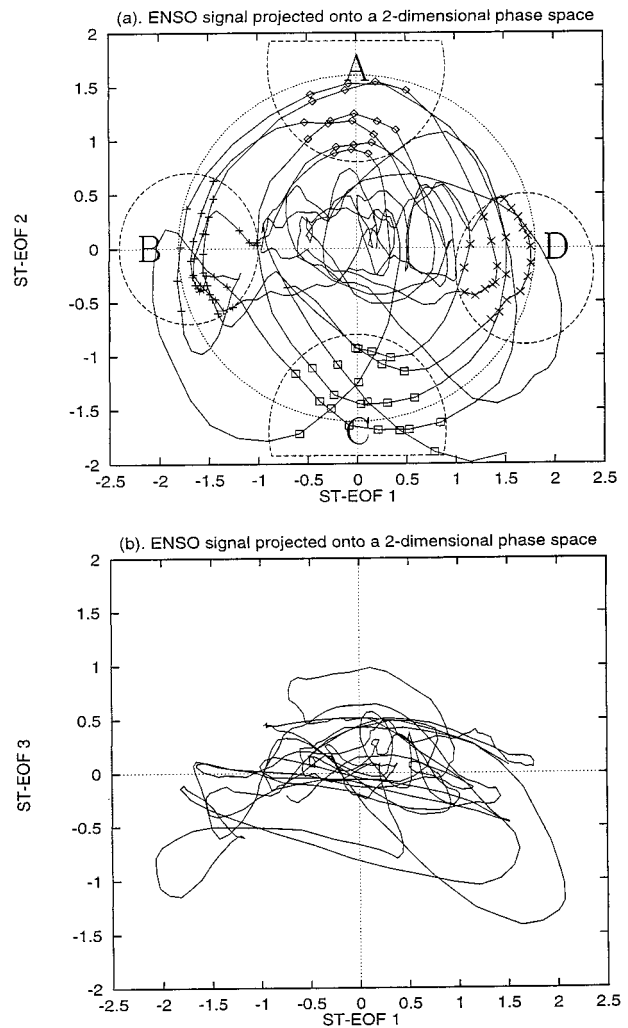

FIG. 7. (a). Phase portrait of the ENSO signal on (v_1, v_2) plane, obtained by plotting y_1 against y_2 (Fig. 5). Marked are the positions representing four typical phases of ENSO time evolution A → B → C → D → A. (b). The same as (a) except on the (v_1, v_3) plane.

events occurred. In both cases, the amplitude of y_3 reaches the minimum. However, they belong to different regimes of the interdecadal changes (see Wang 1995a and section 5c).

To summarize, the first two ST-EOFs (Fig. 4) with their clear indication of phase shift of $\pi/2$, and their associated ST-PCs (Fig. 5), with time shift of a quarter of the typical ENSO life cycle, describe a westward propagation of the SST anomaly associated with El Niño and La Niña in the development of warm or cold episodes (Fig. 7a). This is a dominant feature for most of the ENSO events, especially before 1977. The SST anomaly associated with the events after 1977 is primarily stationary or has an eastward propagation (1982–83). The v_3 contains a structure with both symmetric and antisymmetric components. These three ST-EOFs, together with their ST-PCs, do give a full picture of the

evolution of the SST anomaly associated with the ENSO life cycle, and adding more EOF modes does not provide significant new information. Thus we conclude that a three-dimensional phase space suffices to explain the regularity and aperiodicity of the observed ENSO dynamics. In order to show that the primary features of the observed ENSO are indeed contained in this three-dimensional phase space, we have reconstructed a Hovmöller diagram along the equator based on these three ST-EOFs and ST-PCs, as in Fraedrich et al. (1993). It is found that the propagation of the SST anomaly in physical space is faithfully represented compared to the observed, in particular, with respect to the westward propagation of the normal El Niño evens and the eastward propagation of the special event during 1982–83.

c. Dimensionality of the ENSO signals

Wang and Fang (1996) demonstrated that the Cane–Zebiak (Zebiak and Cane 1987) coupled ocean–atmosphere model essentially consists of only two prognostic equations: the mixed-layer thermodynamics equation for SST and the thermocline depth equation for upper-ocean dynamics. Along with the SST–gradient-wind relation and the wind–equatorial upwelling relation, they compose a closed coupled system. By considering only the largest-scale, equatorial symmetric, standing basin mode, the coupled system reduces to a minimum dynamic system, comparable to the Lorenz model (1963), which highlights the cyclic, chaotic, and season-dependent evolution of ENSO. They show that for a steady annual mean basic state, the dynamic system exhibits a unique limit cycle solution for a fairly restricted range of air–sea coupling. The limit cycle is a stable attractor and represents an intrinsic interannual oscillation of the coupled system. The deepening (shoaling) of the thermocline in the eastern (western) Pacific leads eastern Pacific warming by a small fraction of the cycle, which agrees well with observations. When the basic state undergoes an annual variation, the limit cycle develops into a chaotic attractor and the inherent interannual oscillation displays a low-order deterministic chaos. On the other hand, the transition phase of the oscillation tends to frequently occur in boreal spring when the basic state is most unstable. It was argued that the season-dependent coupled instability may be responsible for the tendencies of ENSO phase locking to the annual cycle and period locking to the integer multiples of the annual period that, in turn, generates irregularities in the oscillation period and amplitude. Using SST time series derived from the Cane–Zebiak model, Tziperman et al. (1995) found that the irregularity of the model ENSO cycle can be explained by the existence of a strange attractor with a fractal dimension (specifically, correlation dimension) of 3.5. The nonlinear time series analysis performed by Chang et al. (1995) reveals that the fractal dimension of their model ENSO dynamics is about 5.2. Both studies suggest that in these models

the irregularity of ENSO is governed by low-order chaotic processes. In an attempt to examine a possible existence of strange attractor for ENSO, Hense (1986) used precipitation at Nauru, SST at Pueto Chicama, and sea level pressure at Darwin to estimate its fractal dimension. Due to the limitation of data both in quantity and in quality, the estimates may not be accurate or reliable (Smith 1988; Eckmann and Ruelle 1992; Fraedrich and Wang 1993). Nevertheless, his estimate of fractal dimension was between 2 and 6.

Thus both statistical estimates and dynamic model studies suggest that the underlying dynamics of ENSO signal is a low-dimensional attractor. It may not be plausible to estimate the exact dimensionality based on observational data (Smith 1988; Eckmann and Ruelle 1992). Our analysis in the previous section indeed indicates that a three-dimensional phase space seems to be sufficient to describe the ENSO signals. In many practical instances, it is often not necessary to know the exact number of a fractal dimension. Instead, it is more important to know the minimum number of coordinates, the so-called embedding dimension, to sufficiently describe the time evolution of the system for theoretical as well as practical purposes, such as the issues of prediction.

5. Phase space characteristics

a. ENSO life cycle

Figure 7 shows that El Niño and La Niña represent the opposite phase of the same wave motion with their mature phases occupying, respectively, the positive and the negative ends of the abscissa (y_1). From the ST–EOF patterns (Fig. 4) we can see that there is a one-to-one correspondence between the direction of the propagation of the SST anomaly in physical space and the speed with which the trajectory rotates around its center (the climate mean) in the phase space (see, e.g., Wallace et al. 1993; Wang et al. 1995). Thus each orbit of the rotating trajectory represents one life cycle of the ENSO. Although each cycle is different, we can portrait the mean life cycle of the ENSO by composite maps of all those monthly SSTs (from different years) that are found in the neighborhood of each typical phase indicated by small circles in the two-dimensional phase space (Fig. 7a). Note that we did not consider v_3 in the searching for the neighbors, as v_3 (and y_3) represents a variability not typical to the ENSO life cycle (see Figs. 4 and 6).

Figures 8a–d show the resulting composite phases in physical space representing the transition from El Niño to La Niña (A), the mature phase of La Niña (B), its transition to El Niño (C), and the mature phase of El Niño (D), respectively. The circle (A → B → C → D → A) gives an ideal picture of the basic evolution of the ENSO life cycle for which any successful dynamic model should be able to reproduce, including the typical wave motion with no particular sign of symmetry of the
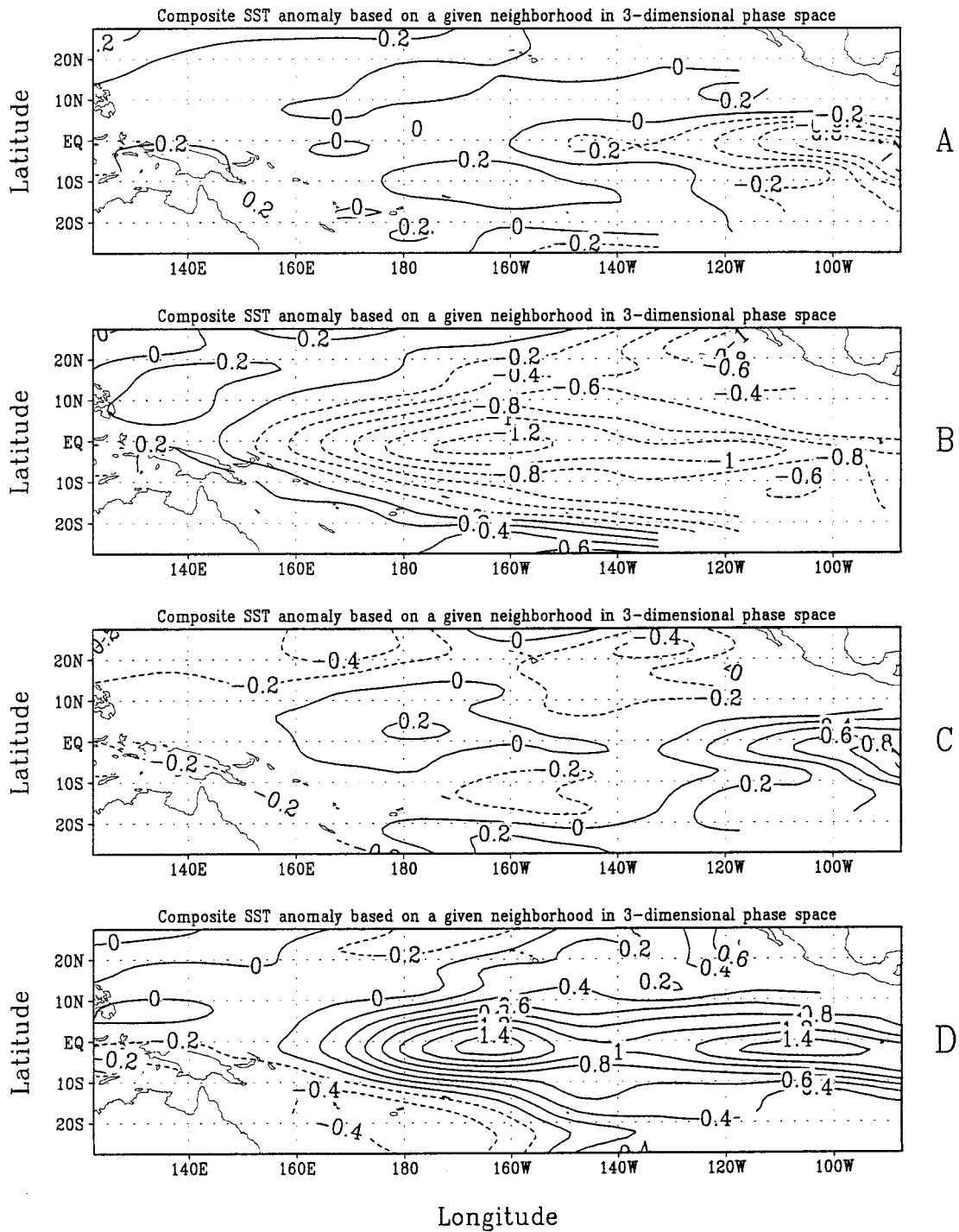
FIG. 8. The SST anomaly associated with the four typical ENSO phases derived from the composite maps of the monthly SST anomalies that fall in each of the four neighborhoods indicated in Fig. 7, representing four different phases of El Niño–La Niña evolution.

opposite phases (Fig. 8). Note that the mature phase of El Niño features two positive SST anomaly centers: one is located in the eastern Pacific (105°W) and the other in the central Pacific (160°W).

b. Phase locking to the annual cycle

The second feature of the ENSO dynamics is its phase locking to the annual cycle (Rasmusson et al. 1990).

FIG. 9. The same as Fig. 7 except that the positions for each month of each year in (a) autumn (SON), (b) winter (DJF), (c) spring (MAM), and (d) summer (JJA) are marked in order to show the phase locking to the annual cycle and their seasonal changes (see text).

This is most clearly revealed in Fig. 9, which is the same as Fig. 7a but marked with the position of each month for each year (see also Fig 3). Note that Figs. 9a–d give the position of the months in spring, summer, autumn, and winter, respectively. For instance, Fig. 9a is marked with the location of March, April, and May on the trajectory to show if there is a preferred clustering of the states according to season due to the phase locking to the annual cycle. It is apparent that the phase locking occurs only when the ENSO signals are relatively strong. In contrast, no preference of seasonal distribution can be observed when the ENSO signal is weak, that is, when the SST distribution is close to climate mean (ST-PCs $\sim$ 0). There is a spring preference in the transition phases (Fig. 9a). The most apparent phase locking occurs in boreal autumn–winter seasons (Figs. 9c,d, particularly in boreal autumn months) for both warm (El Niño) and cold (La Niña) events. Note that the phase locking often occurs in opposite phases along

a straight line, differing by 180° of phase angle or half of the typical ENSO life cycle, which gives rise to the biennial component of the ENSO cycle observed in Rasmusson et al. (1990).

c. Irregularity

The phase portraits (see Figs. 3 and 7) show two basic features of the orbit structure. First, the center of orbits changes its position from one orbit to another. This is often associated with the regime behavior that gives rise to variabilities with timescales longer than a typical ENSO life cycle. The observed interdecadal variability in y_3 is not independent from this regime behavior. Second, each orbit (ENSO life cycle) differs from the other in terms of intensity, phase locking to the annual cycle, and phase speed (equivalent to SST anomaly propagation in physical space). Thus the ENSO variability is characterized by both periodicity (different from Ran-
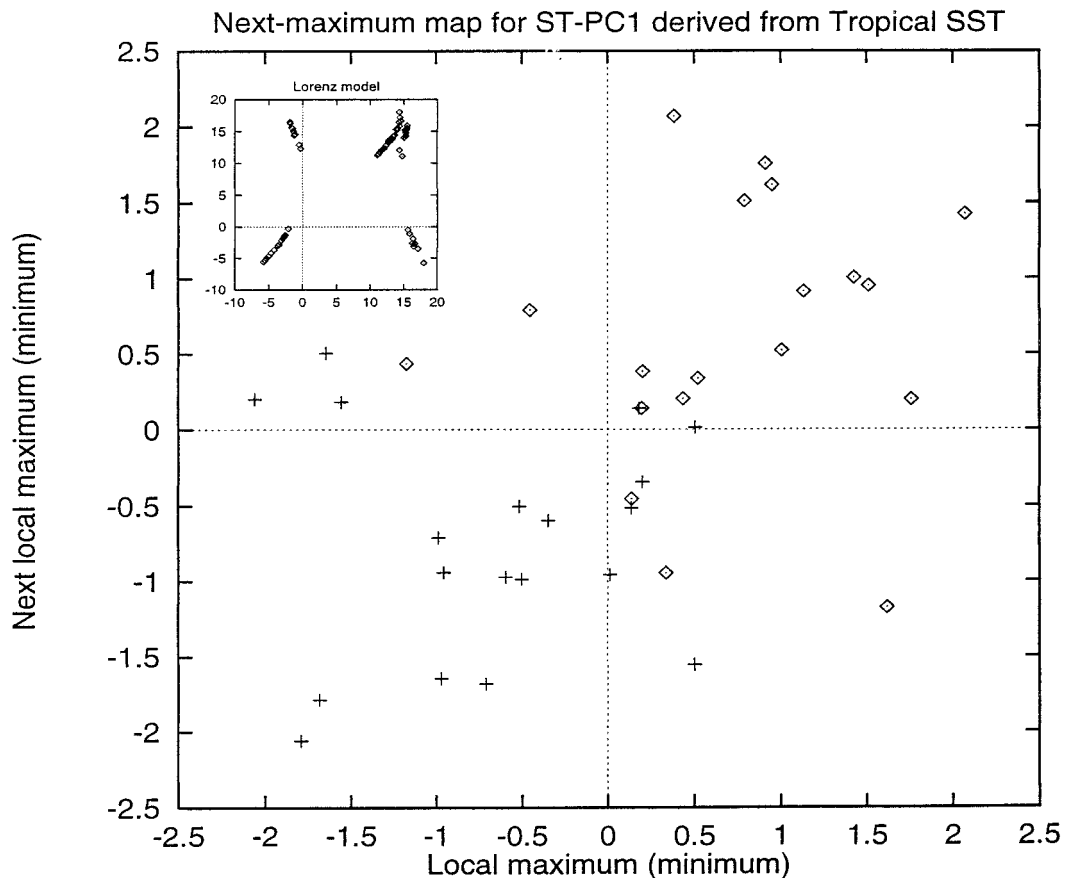
FIG. 10. First return map obtained by plotting a local maximum of ST-PC$_1$ (see Fig. 5) against its next as well as the local minimum against the next minimum. Both are equivalent to a Poincaré section. For comparison, the same map derived from the Lorenz model is given in the upper-left corner, as in Fig. 11.

dom processes) and irregularity (similar to random processes). This structured variability, often referred to as aperiodicity to distinguish from randomness, can conveniently be quantified in terms of phase space representation.

To study the regime behavior, one needs to calculate the probability density distribution or Poincaré section. This is too hard a task for the present study due to the limitation of data. We can gain some qualitative knowledge based on the above observation about the regime behavior. For a supplementary evidence, we tentatively give the first return map of the ENSO signal in Fig. 10 obtained by plotting a local maximum of the y_1 against its next maximum. This is equivalent to a Poincaré section showing whether there is a preferred clustering of the orbits of the trajectories. Albeit the limited number of orbits, Fig. 10 seems to indicate that there is a preferred distribution of the orbits, in contrast to random processes. However, the distribution is more complex than a typical theoretical low-dimensional model, such as the Lorenz (1963) model, which is given on the upper left corner of the figure for comparison. This situation seems to be typical of reality, which gives the hope and,

at the same time, the limitation for some practical issues such the ENSO prediction.

To quantify the properties associated with the ENSO activity and phase propagation, we calculated the amplitude of the wave intensity defined by the radius of the orbit ($r = (y_1^2 + y_2^2)^{1/2}$) and the phase speed ($\theta = d_\phi/d_t$), where ϕ is the phase in degree with respect to the initial position $\phi = 0°$. Details about the method of calculation are referred to Wallace et al. (1993) and Wang et al. (1995). Figure 11a (upper panel) shows the results: the ENSO intensity displays an apparent irregularity, similar to intermittency, whose gross feature is quite comparable to the well-known Lorenz model shown on the upper left corner of the figure (see Lorenz 1963 for details). The calculation is based on two-dimensional (dashed line) and three-dimensional (solid line) phase spaces. Note that inclusion of y_3 does not influence the qualitative feature of the ENSO intensity, implying that v_3 is not essential to the typical ENSO life cycle, but more related to the changes among the life cycles, typically, the interdecadal changes. There seem to be both regime behavior and intermittence associated with the interdecadal changes: for instance,
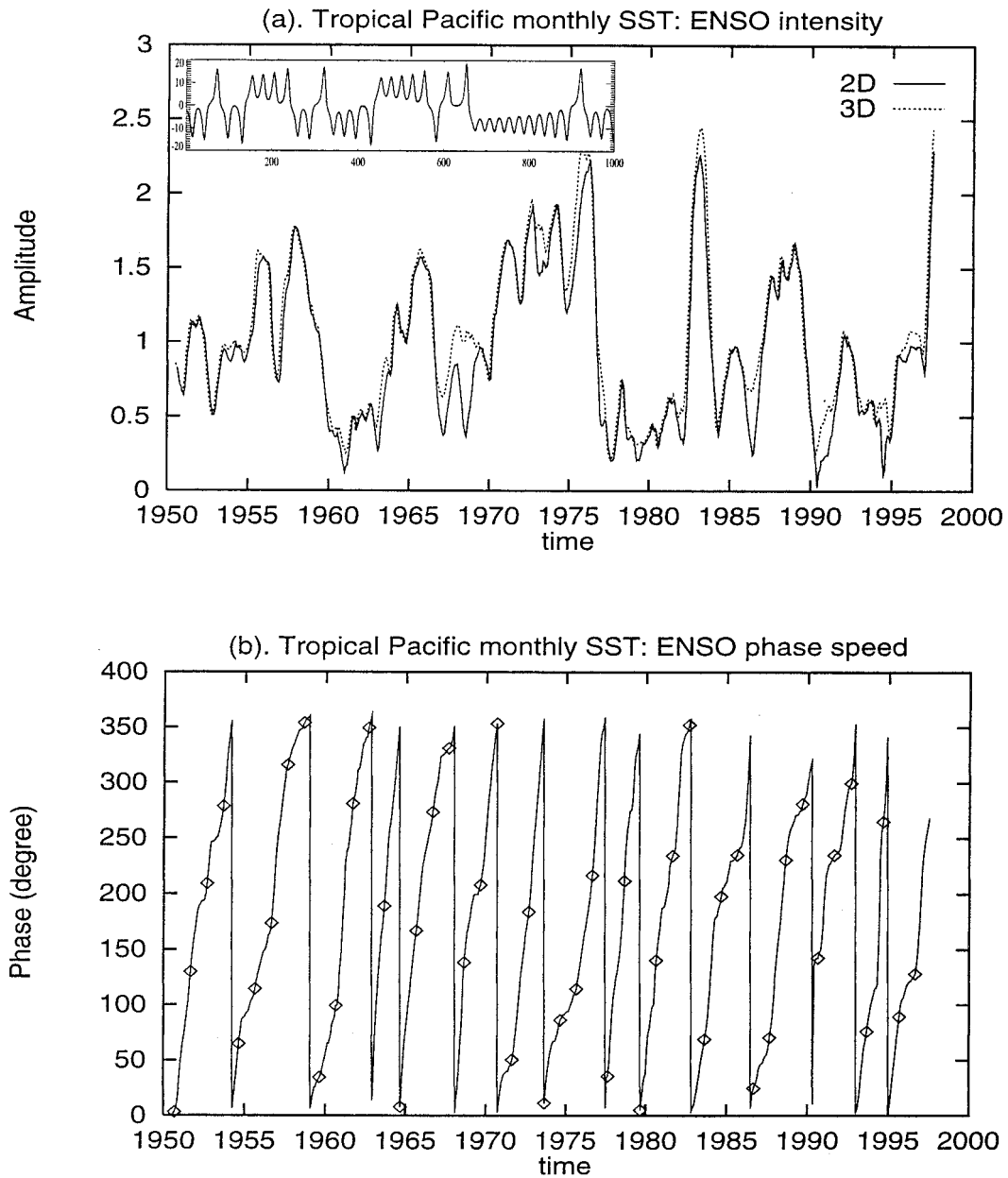
FIG. 11. (a) Intensity of the ENSO activity defined as the radius of the trajectory in the two-dimensional [(v_1, v_2), dashed line] and three-dimensional [(v_1, v_2, v_3), solid line] phase space, respectively. (b) The phase position (in degrees) of the ENSO state in the (v_1, v_2) plane (see Fig. 7a). Marked are the positions for each September in order to show the phase locking for each ENSO life cycle.

from 1970 to 1976 there are intensive ENSO signals (El Niño–La Niña events), followed by a period (1977–81) when there is almost no signal. For convenience, a period with almost no ENSO signal is referred here as a "quiet period." A long and extraordinarily quiet period, such as the first halves of the 1970s and 1990s, is often followed by a burst of drastic single El Niño event, such as those in 1982–83 and 1997–98. A shorter quiet period often preludes relative weaker ENSO signals, resulting in more frequent occurrences of the El Niño–La Niña events, such as the period from the mid-1960s to the

mid-1970s. These qualitative features are in agreement with the observations from the wavelet analysis results (Wang and Wang 1996).

The phase propagation, together with the position of September each year, is shown in the lower panel of Fig. 11 by plotting the phase position in degree (ϕ) for each ENSO life cycle ($0° \leq \phi \leq 360°$). The position of September serves as an indicator about the number of annual cycle within each ENSO life cycle. September is chosen to be the indicator here because this is the month during which the eastern Pacific cold tongue of

SST reaches its maximum (e.g., B. Wang 1994). The phase speed (θ) is measured by the slope of the ϕ curve for each cycle. Three basic features can be detected as follows.

First, the phase propagation changes from cycle to cycle and there is almost no smooth propagation. Apparent stalls can be observed for most of the ENSO life cycles (11 out of 15).

Second, the typical life cycle of the ENSO is, in fact, dominated by a period of 4 yr. There are cycles when the period is 2, 3, or 5 yr. The biennial cycle (2–3 yr) appears to be significant in mid-1960s (Fig. 11b). Those observed in the late 1970 is not typical, as this is the quiet period of the ENSO signal (see Fig. 11a). Apart from these two periods, the majority of the ENSO cycles are 4 yr. In this sense, the biennial component observed in spectral analysis may simply come from a subharmonic of the 4-yr ENSO life cycle. In particular, the mature phases tend to be locked to boreal winter and the associated transition phases are rapid. These two features combined together may lead to an "apparent" biennial peak in spectral analysis. A typical example is the event in 1982–83 when the warm phase developed in May 1982 and decayed July 1983. Figure 11b shows that this component is only a part of the ENSO life cycle. Here one may need to distinguish the different types of biennial components: the component that is a part of the ENSO signals and the component observed during the quiet periods. The latter component may be due to the influences from some other sources of variabilities such as the biennial variability of the tropical circulation system, in particular, the monsoon variability. The classic spectral analysis cannot tell these differences.

Third, the stall of propagation has a preferred phase positions and seasons. This is related in part with the phase locking to the annual cycle, which becomes immediately apparent when one examines the phase distribution of the Septembers: about one-half falls in the narrow range of 340°–90°. The other half tend to fall in 100°–200° for the pre-1970 epoch and 200°–300° in the post-1970 period. These again are related to the regime behavior of the ENSO dynamics and its interdecadal changes.

6. Concluding remarks

The foregoing analysis leads to the conclusion that the essential part of the observed ENSO variability is equivalent to a low-dimensional attractor, as contrast to pure stochastic processes. The three-dimensional basis, (v_1, v_2, v_3), derived from the ST-EOFs of the monthly mean SST of the tropical Pacific, can effectively describe the basic features of the observed variability, such as the irregular oscillation, the phase locking to the annual cycle and the interdecadal variations in its propagation and onset. Adding further dimension does not

increase any significant new information about the underlying dynamics.

The phase–space analysis of the ENSO variabilities reveals that El Niño and La Niña are two extreme phases of the same phenomenon with a typical life cycle of about 4 yr, referred to as the ENSO signal. The mature phases tend to occur in boreal winter and the associated transition phases are rapid. The phase locking to the annual cycle took place only when ENSO signals are relatively strong while the most significant phase locking occurs in boreal autumn and winter. All these factors leads to an apparent biennial peak in spectral analysis. However, there is another biennial component observed during the periods when there are no ENSO signals or the ENSO signals are very week, that is, the quiet period. This biennial component has a very different origin as that of the ENSO signal. The classical spectral analysis cannot distinguish these two different components.

There is a preferred distribution of the orbits of the ENSO signals in contrast to random processes. Thus the variability of the ENSO signals is apparently structured but changes from one life cycle to another. The intensity and the frequency of occurrences of the El Niño–La Niña events display an irregularity with the regime behavior and intermittency comparable to the Lorenz (1963) set, which constitutes the major part of the observed interdecadal variability. The physical aspects of interdecadal component, represented by v_3 and y_3, display the same characteristics as discussed in Wang (1995a). Our analysis shows that the interdecadal variability is a complex regime behavior reflected by the onset of the ENSO events (phase relation of the three ST-PCs), the length of the ENSO life cycle, the intermittency, and the ENSO intensity (Fig. 11).

Regarding the above conclusion, we should like to make the following comments. First, the existence of a low-dimensional phase space for a complex system is the key to the conceptual understanding of the underlying dynamics and possibly leads to effective prediction of its long-time behavior. However, direct estimation of dimensionality, which requires a large quantity of data with good quality (Smith 1988; Sauer et al. 1991), is often less plausible when dealing with observed physical systems. In practice, we may not need to know the fractal dimensions when dealing with dynamic systems of the physical reality. It may be indeed more useful to know the minimum number of coordinates that can effectively describe the observed variabilties. Therefore, the conclusion regarding the dimensionality of the El Niño–La Niña is based on the physical insight derived from observational studies and the theoretical models of the underlying system rather than from estimating the fractal dimensions. On the one hand, three-dimensional basis is indeed able to capture the observed features. On the other hand, the dynamic system models (Wang and Fang 1996) and the coupled numerical model results (Tziperman et al. 1995; Chang et al. 1995) also suggest that the basic dynamics gov-

erning the evolution of the ENSO signals is a low-dimensional chaotic attractor. Thus, the ENSO signals provides an example of a complex system of the coupled ocean and atmosphere generating relatively simple dynamics in terms of a low dimensionality.

Second, the phase space analysis of such a low-dimensional system can often reveal the detailed structure of the observed variabilities of the ENSO signal: its life cycle and its irregularity. This implies that any numerical model should be able to recreate both the observed low-dimensional attractor and the observed structures and dynamic behavior, if they have the right physics. Comparison of the classic statistic quantities, such as means, variances, correlations, and spectra, may be insufficient to validate a numerical model.

REFERENCES

Abarbanel, H. D. I., R. Brown, J. J. Sidorowich, and L. S. Tsimring, 1993: The analysis of observed chaotic data in physical systems. *Rev. Mod. Phys., 65* (4), 1331–1392.

Broomhead, D. S., and G. P. King, 1986: Extracting qualitative dynamics from experimental data. *Physica D, 20,* 217–236.

Chang, P., L. Ji, B. Wang, and T. Li, 1995: Interaction between the seasonal cycle and El Niño–Southern Oscillation in an intermediate coupled ocean–atmosphere model. *J. Atmos. Sci., 52,* 2353–2372.

Deser, C., and J. M. Wallace, 1987: El Niño events and their relation to the Southern Oscillation: 1925–1986. *J. Geophys. Res., 92,* 14 189–14 196.

——, and ——, 1990: Large-scale circulation features of warm and cold episodes in the tropical Pacific. *J. Climate, 3,* 1254–1281.

Eckmann, J. P., and D. Ruelle, 1985: Ergodic theory of chaos and strange attractors. *Rev. Mod. Phys., 57,* 617–656.

——, and ——, 1992: Fundamental limitations for estimating dimensions and Lyapunov exponents in dynamical systems. *Physica D, 56,* 185.

Fraedrich, K., 1986: Estimating the dimensions of weather and climate attractors. *J. Atmos. Sci., 43,* 419–432.

——, and R. Wang, 1993: Estimating the correlation dimension from noisy and small data set based on re-embedding. *Physica D, 65,* 373–398.

——, ——, and S. Pawson, 1993: An EOF analysis of the vertical-time-delay structre of the quasibiennial oscillation (QBO). *J. Atmos. Sci., 50,* 3357–3365.

Guckenheimer, J., and P. Holmes, 1983: *Nonlinear Oscillations, Dynamical Systems, and Bifurcations of Vector Fields.* Vol. 42, *Applied Mathematical Sciences,* Springer-Verlag, 453 pp.

Hense, A., 1986: On the possible existence of a strange attractor for the Southern Oscillation. *Beitr. Phys. Atmos., 60,* 34–47.

Jin, F.-F., D. Neelin, and M. Ghil, 1994: El Niño on the devil's staircase: Annual subharmonic steps to chaos. *Science, 264,* 70–72.

Lorenz, E. N., 1963: Deterministic nonperiodic flow. *J. Atmos. Sci., 20,* 130–141.

Neelin, J. D., M. Latif, and F.-F. Jin, 1994: Dynamics of coupled ocean–atmosphere models: The tropical problem. *Ann. Rev. Fluid Mech., 26,* 617–659.

Nitta, T., and S. Yamad, 1989: Recent warming of tropical sea surface temperature and its relationship to the Northern Hemisphere circulation. *J. Meteor. Soc. Japan, 67,* 375–383.

Philander, S. G., 1990: *El Niño, La Niña, and the Southern Oscillation.* Academic Press, 293 pp.

Plaut, G., and R. Vautard, 1994: Spells of low-frequency oscillations and weather regimes in the Northern Hemisphere. *J. Atmos. Sci., 51,* 210–236.

Rasmusson, E. M., and T. H. Carpenter, 1982: Variation in tropical sea surface temperature and surface wind fields associated with the Southern Oscillation/El Niño. *Mon. Wea. Rev., 110,* 354–384.

——, X. Wang, and C. F. Ropelewski, 1990: The biennial component of ENSO variability. *J. Marine Syst., 1,* 71–96.

Sauer, T., J. A. Yorke, and M. Casdagli, 1991: Embedology. *J. Statis. Phys., 65,* 579–616.

Smith, L. A., 1988: Intrinsic limits on dimension calculations. *Phys. Lett., 133A,* 283.

Smith, T. M., R. W. Reynolds, and C. F. Ropelewski, 1994: Optimal averaging of seasonal surface temperatures and associated confidence intervals (1860–1989). *J. Climate, 7,* 949–964.

Takens, F., 1981: Detecting strange attractors in turbulence. *Proceedings of Warick Symposium 1980,* D. A. Rand and L.-S. Young, Eds., Springer Verlag, 366–381.

Trenberth, K. E., and D. J. Shea, 1987: On the evolution of the Southern Oscillation. *Mon. Wea. Rev., 115,* 3078–3096.

Tziperman, E., M. A. Cane, and S. E. Zebiak, 1995: Irregularity and locking to the seasonal cycle in an ENSO prediction model as explained by the quasi-periodicity route to chaos. *J. Atmos. Sci., 52,* 293–306.

Vallis, G. K., 1986: El Niño: A chaotic dynamical system? *Science, 232,* 343–245.

——, 1988: Conceptual model of El Niño and the Southern Oscillation. *J. Geophys. Res., 93* (C), 13 979–13 991.

——, C. Pires, and G. Plaut, 1996: Long-range atmospheric predictability using space–time principal components. *Mon. Wea. Rev., 124,* 288–307.

Wallace, J. M., L. Panetta, and J. Estberg, 1993: A phase-space representation of the equatorial stratospheric quasi-biennial oscillation. *J. Atmos. Sci., 50,* 1751–1762.

Wang, B., 1994: On the annual cycle in the tropical eastern central Pacific. *J. Climate, 7,* 1926–1942.

——, 1995a: Interdecadal changes in El Niño onset in the last four decades. *J. Climate, 8,* 267–285.

——, 1995b: Transition from a cold to a warm state of El Niño–Southern Oscillation cycle. *Meteor. Atmos. Phys., 56,* 17–32.

——, and Y. Wang, 1996: Temporal structure of the Southern Oscillation as revealed by waveform and wavelet analysis. *J. Climate, 9,* 1586–1598.

——, and Z. Fang, 1996: Chaotic oscillation of the tropical climate: A dynamic system theory for ENSO. *J. Atmos. Sci., 53,* 2786–2802.

——, A. Barcilon, and Z. Fang, 1998: Stochastic dynamics of El Niño–Southern Oscillation. *J. Atmos. Sci., 56,* 5–23.

Wang, R., 1991: Propagating waves in the EOF-decomposition of space–time-delay diagrams. *Ann. Geophys., 9,* C588–C599.

——, 1994: *A Phase-Space Approach to Atmospheric Dynamics Based on Observational Data—Theory and Applications.* Me-

teor. Abhandl. (Neue Folge), A8(2), Verlag von Dietrich Reimer, 227 pp.

——, K. Fraedrich, and S. Pawson, 1995: Phase-space characteristics of the tropical stratospheric quasi-biennial oscillation. *J. Atmos. Sci.,* **52,** 4482–4500.

Weare, B. C., and J. S. Nasstrom, 1982: Examples of extended empirical orthogonal function analysis. *Mon. Wea. Rev.,* **110,** 481–485.

Whitney, H., 1936: Differentiable manifolds. *Ann. Math.,* **37,** 645–680.

Woodruff, S. D., R. L. Jenne, and P. M. Steurer, 1987: A comprehensive ocean–atmosphere dataset. *Bull. Amer. Meteor. Soc.,* **68,** 1239–1250.

Wright, P. B., J. M. Wallace, T. P. Mitchell, and C. Deser, 1988: Correlation structure of the El Niño/Southern Oscillation phenomenon. *J. Climate,* **1,** 609–625.

Zebiak, S. E., and M. A. Cane, 1987: A model El Niño–Southern Oscillation. *Mon. Wea. Rev.,* **115,** 2262–2278.

Zeng, X., R. A. Pielke, and R. Eykholt, 1993: Chaos theory and its applications to the atmosphere. *Bull. Amer. Meteor. Soc.,* **74,** 631–644.